Dipeptide self-assembly into water-channels and gel biomaterial†

Ottavia Bellotto, [a] Giovanni Pierri, [b] Petr Rozhin, [a] Maurizio Polentarutti,[c] Slavko Kralj, [d,e] Paola D'Andrea,[f] Consiglia Tedesco *[b] and Silvia Marchesan *[a]

Dipeptides are convenient building blocks for supramolecular gel biomaterials that can be produced on a large scale at low cost and do not persist in the environment. In the case of unprotected sequences, hydrophobicity is a key requirement to enable gelation, with Phe–Phe standing out for its self-assembling ability. Conversely, more hydrophilic sequences such as homochiral dipeptides Phe–Val and Val–Phe neither fibrillate nor gel aqueous buffers and their crystal structures reveal amphipathic layers. In this work, we test emerging rules for the design of self-assembling dipeptides using heterochiral Phe–Val and Val–Phe. Each dipeptide is characterized by ^{1}H- and ^{13}C-NMR, LC-MS, circular dichroism, infrared and Raman spectroscopies, rheology, electron microscopy, and single-crystal X-ray diffraction. In particular, D-Phe–L-Val is the first heterochiral dipeptide to self-assemble into supramolecular water-channels whose cavity is defined by four peptide molecules arranged head-to-tail. This minimalistic sequence is devoid of amyloid character as probed by thioflavin T fluorescence and it displays excellent biocompatibility *in vitro*. The dataset provided, through comparison with the literature, significantly advances the definition of molecular design rules for minimalistic unprotected dipeptides that self-assemble into water-channels and biocompatible gels, to assist with the future development of supramolecular biomaterials with fine control over nanomorphological features for a variety of applications.

Introduction

Short peptides have become very popular building blocks for supramolecular materials that can be formed in water and other green solvents, on a large scale at low cost, and that do not persist in the environment.[1] In particular, dipeptides are the simplest building blocks of this class of biomolecules, thus being the most advantageous in terms of ease of preparation and production cost, both of which are key to enable their translation into commercial products.[2,3] Potential fields of applications are numerous and very diverse, and they range from medicine,[4–7] to bioelectronics,[8–10] and energy.[11,12]

However, it is well-known that prediction of supramolecular behaviour of dipeptides is very challenging, owing to their richness in available conformations, and diversity in their functional groups, so that even subtle structural differences are amplified through cooperative self-assembly, into dramatically different outcomes.[13–15] The most widely used strategy in their design is based on the use of polyaromatic N-caps, which can easily stack and drive self-aggregation.[13,16] Conversely, unprotected dipeptides are more unpredictable in terms of their ability to self-organize into defined nanomorphologies to enable hierarchical assembly into macroscopic materials.

Our group has become interested in the supramolecular effects of amino acid chirality, to use it as a means to control short peptide self-assembly. If we consider linear dipeptides composed of natural amino acids without further chemical modifications, Phe–Phe stands out for its remarkable propensity to self-organize into a variety of nanomorphologies, especially nanotubes and fibers.[17–19] Unfortunately, often this process allows little control over hierarchical assembly at the microscale, with heterogeneous sizes of Phe–Phe assemblies that can be toxic to cells.[20,21] Conversely, a change in stereoconfiguration at a single carbon atom to heterochiral D-Phe–L-Phe surprisingly maintained its ability to pack into nanotubes.

[a]University of Trieste, Chem. Pharm. Sc. Dept., Via Giorgieri 1, 34127 Trieste, Italy. E-mail: smarchesan@units.it
[b]University of Salerno, Dept. of Chemistry & Biologi "A. Zambelli", Via Giovanni Paolo II 132, 84084 Fisciano, SA, Italy. E-mail: ctedesco@unisa.it
[c]Elettra-Sincrotrone Trieste, S.S. 114 km 163.5, Basovizza, 34149 Trieste, Italy
[d]Jožef Stefan Institute, Materials Synthesis Dept., Jamova 39, 1000 Ljubljana, Slovenia
[e]University of Ljubljana, Pharmaceutical Technology Dept., Faculty of Pharmacy, Aškerčeva 7, 1000 Ljubljana, Slovenia
[f]University of Trieste, Life Sciences Dept., Via L. Giorgieri 5, 34127 Trieste, Italy

†Electronic supplementary information (ESI) available: spectroscopy, rheology, microscopy, photographs, single-crystal XRD data. CCDC 2160976 and 2160978. For ESI and crystallographic data in CIF or other electronic format see DOI: https://doi.org/10.1039/d2ob00622g

However, it suppressed hierarchical bundling as it enabled intramolecular face-to-face aromatic interactions at the expense of intermolecular ones. In this way, double-layered peptide nanotubes were stabilised and yielded clear gels.[20]

An unanswered question remained the elucidation of structural rules to enable the formation of water-filled nanotubes and macroscopic hydrogels from dipeptides containing also hydrophobic amino acids other than Phe, such as the aliphatic Ala, Val, Ile, and Leu. To gain knowledge in this area, we recently studied all possible stereoisomer and regioisomer combinations of Phe with either Leu or Ile. It was noted that heterochirality increased hydrophobicity and favoured assembly into crystals or hydrogels, as shown on dipeptides bearing Leu/Ile and Phe amino acids. However, the formation of water-filled nanotubes with a cavity defined by six peptide molecules connected head-to-tail, as with Phe–Phe, was confirmed only for one compound out of 8, *i.e.*, D-Phe–L-Ile.[22,23]

Water-filled nanotubes are particularly interesting as they could potentially insert into membranes and alter cell permeability. Phe–Phe was indeed shown to do so selectively on bacteria, thus exerting an antimicrobial effect.[24] Stacks of cyclopeptides into nanotubes were also effectively used to the same end.[25,26] Furthermore, applications can go well beyond the treatment of infections. For instance, they have shown proton conductivity both in the wet and dry state, a property that could be useful to develop innovative, green devices for energy storage and conversion that do not persist in the environment.[27] To this end, the formation of water-channels in crystalline structures obtained from simple, linear, short peptides is very attractive, and was successfully demonstrated to display evaporation-induced actuation.[28] However, design rules to understand which short sequences can form water-channels, and which don't, are still lacking.

To shed light on this unanswered question, in this work we studied the self-assembly behaviour of heterochiral Val–Phe and Phe–Val. Valine shares the feature of a β-branched hydrophobic sidechain with Ile and Phe, and both D-Phe–L-Ile (but not D-Ile–L-Phe)[22] and D-Phe–L-Phe[20] maintained the ability to self-assemble into water-filled nanotubes. Previous studies on homochiral Val–Phe[29] and Phe–Val[30] revealed no fibrillation, and their crystal structures were formed by amphipathic layers,[31,32] devoid of water-channels. However, heterochirality was shown to increase dipeptide hydrophobicity, relative to homochiral stereoisomers, and promote fibrillation in aqueous solutions,[22,23] thus giving scope for the present study.

Results and discussion

Synthesis and molecular characterization

The four possible heterochiral dipeptides from Val and Phe are shown in Scheme 1. Enantiomers display identical supramolecular behaviour in achiral environments, therefore D-Phe–L-Val and D-Val–L-Phe (left in Scheme 1) are representatives of the four enantiomeric pairs. They were synthesised by standard solid-phase methods, purified by HPLC, and identified by LC-MS, ^{1}H-NMR and ^{13}C-NMR (see ESI, Sections S1–S3).

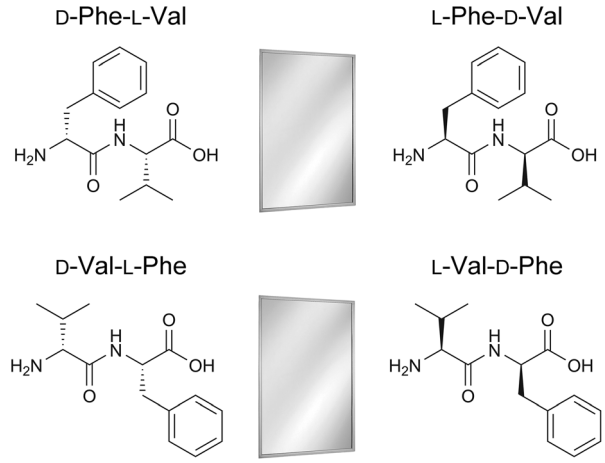

Scheme 1 Chemical structures of the 4 heterochiral dipeptides from Val and Phe.

When analysed by reversed-phase HPLC, the two dipeptides displayed nearly identical retention times (R_t), which can be considered an experimental measure for hydrophobicity.[33] In diluted solutions, the circular dichroism (CD) spectra were reminiscent of their analogues with Ile instead of Val (see ESI, S4†).[22] In all cases, considering that enantiomers are expected to display mirror-imaged CD spectra with opposite ellipticity, we can conclude that the sign of the CD signal above 200 nm is determined by Phe chirality (*i.e.*, negative for D-Phe and positive for L-Phe),[34] regardless of its position along the sequence (*i.e.*, at the N- or C-terminus). This type of CD signature with two peaks at 198 and 218 nm can be representative of a population of conformations, whose majority have dihedral angles typical of β-structures, and which can be found also for non-assembling analogues.[35,36]

Supramolecular studies in phosphate buffered saline (PBS)

The ability to self-assemble and gel was probed by using a standard protocol.[22] The dipeptides were first dissolved in PBS upon heating, and subsequent cooling down to room temperature (Fig. 1A) afforded an opaque gel solely for D-Phe–L-Val (minimum gelling concentration, mgc of 40 mM). Conversely, D-Val–L-Phe rapidly crystallised when tested at concentrations that were higher than its solubility (*i.e.*, 100 mM, Fig. 1B). Optical microscopy images revealed fibers for the former (Fig. 1A), and crystals for the latter (Fig. 1B), which were of suitable quality for single-crystal X-ray diffraction (XRD, *vide infra*). Transmission electron microscopy (TEM) confirmed the presence of fibers for D-Phe–L-Val with a median diameter of ~1 micron (n = 50; Fig. 2A and C). By contrast, D-Val–L-Phe formed amorphous aggregates at the same concentration (Fig. 2B). Interestingly, both compounds tested negative for thioflavin-T (ThT) fluorescence (see ESI, S5†), which is a standard assay used to probe for the presence of amyloids and quantify the critical aggregation concentration.[37] The dye fea-

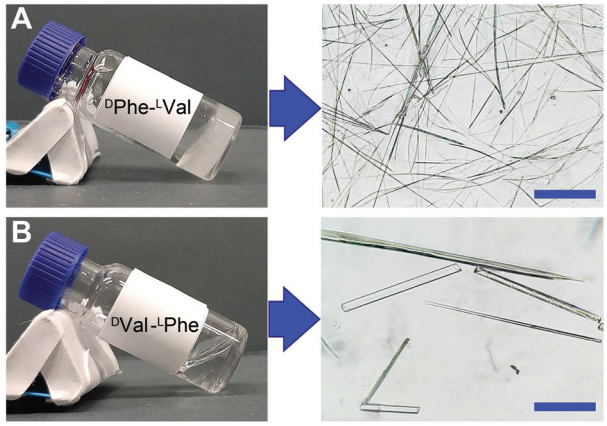

Fig. 1 Photographs and optical microscopy images of (A) D-Phe–L-Val and (B) D-Val–L-Phe in PBS at concentrations above their solubility. Scale bar = 100 μm.

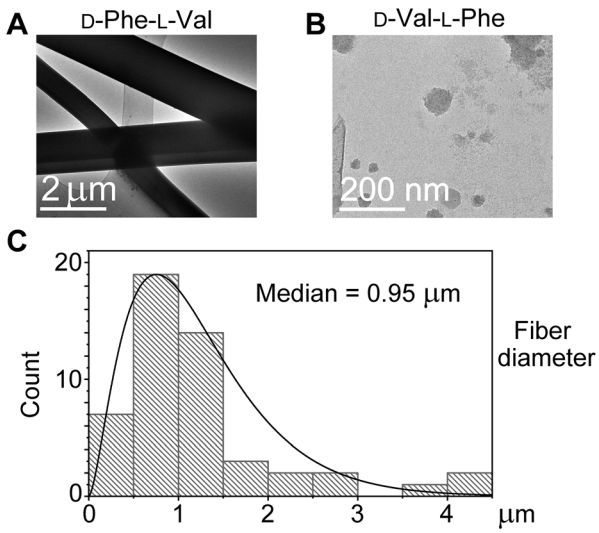

Fig. 2 (A and B) Transmission electron micrographs (TEM) for the two dipeptides revealed microfibers only for D-Phe–L-Val, with a median diameter of ~1 micron (C).

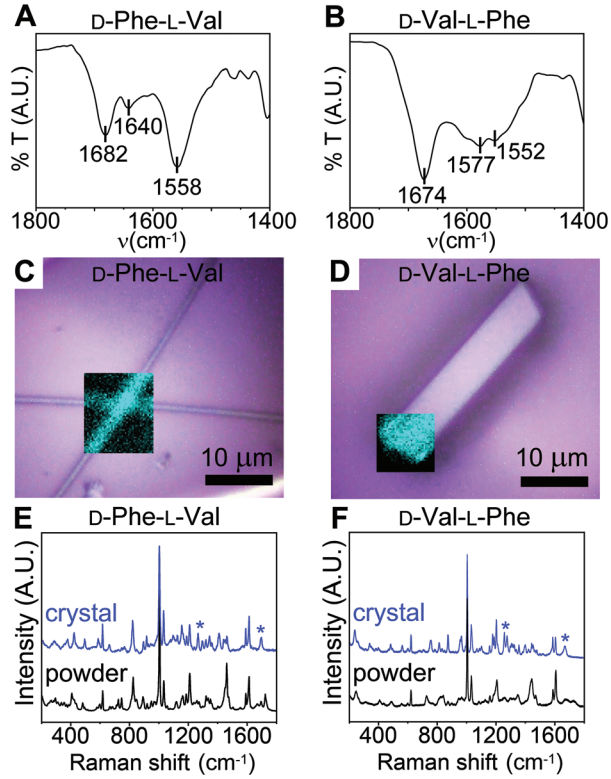

Fig. 3 (A and B) Amide I–II region of the FT-IR spectra of the two samples. (C and D) Raman mapping of the aromatic signal at 1005 cm^{-1} (cyan) overlayed on the optical microscopy images of fibers (C) and crystals (D). (E and F) Raman spectra. Blue asterisks denote signal rising with assembly in the amide I–III region.

tures a benzothiazole moiety linked to a dimethylanilino ring *via* a C–C bond, whose rotation is impeded when the dye binds onto hydrophobic grooves of amyloid fibrils, leading to fluorescence.[38] Considering that D-Phe–L-Val does fibrillate, as confirmed by transmission electron microscopy analysis (Fig. 2A), we can conclude that the topography of its fibers is not suitable for effective binding of ThT. The dye was shown to bind to β-sheets composed of at least four consecutive β-strands,[39] therefore we used Fourier-transformed infrared spectroscopy to analyse the peptide conformation. The amide I and II regions of FT-IR spectra (Fig. 3A and B) revealed sharper peaks for D-Phe–L-Val, relative to D-Val–L-Phe, and this finding can be an indication of the higher supramolecular order of the former relative to the latter. Both compounds displayed peaks in the region where β-turns are found for longer sequences (*i.e.*, 1682 and 1674 cm^{-1}, respectively), as previously found for Ile analogues.[22] However, only gelling D-Phe–L-Val had a signal at 1640 cm^{-1} that is in the range between β-structures and disordered conformations.

Raman microspectroscopy is another useful technique to investigate these systems (Fig. 3C–F). In all cases, spectra were dominated by the aromatic signal at 1005 cm^{-1} that can be used for mapping of the microstructures (Fig. 3C and D). D-Phe–L-Val self-assembly was accompanied by the rising of signals at 1266 cm^{-1} in the amide III region, and 1694 cm^{-1} in the amide I range (Fig. 3E, blue asterisks), as a result of the supramolecular stacking through establishment of H-bonding networks involving the amide bonds. Another signal of interest is at 1294 cm^{-1} that likely corresponds to C–H bending modes.[40] The same set of signals arose with crystallization of D-Val–L-Phe, although in this case they were all downshifted to 1257 cm^{-1}, 1277 cm^{-1}, and 1672 cm^{-1} (Fig. 3F). Upshifts can result from extended H-bonding networks,[20,41] suggesting a more pronounced effect for the gelator D-Phe–L-Val relative to D-Val–L-Phe. Single-crystal XRD structures of hydrophobic dipeptides had shown that in the case of non-gelling isomers water molecules were mediating peptide–peptide H-bonds through the amides, while in the case of gelators, peptide molecules were interacting directly in extended stacks.[22,23] To

verify whether this is a general rule that applies also to D-Phe–L-Val and D-Val–L-Phe, single-crystal XRD analyses were performed.

Single-crystal X-ray diffraction (XRD)

Single-crystal XRD structures of both compounds were solved using synchrotron radiation (Fig. 4, 5 and ESI, Section S6†). D-Phe–L-Val microfibers evolved into crystals over the course of several days. The dipeptide crystallises in a tetragonal unit cell (space group *I*4). Four hydrophobic dipeptides arrange head-to-tail inducing the formation of a hydrophilic amide-rich channel filled with water molecules and a hydrophobic region defined by the aminoacidic sidechains establishing weak hydrophobic interactions (Fig. 4). The channels are parallel to the shortest *c* axis and are filled with water molecules, which do not show full occupancy. According to Görbitz's classification,[42] D-Phe–L-Val can be considered as a member of the Phe–Phe class of dipeptides forming porous structures. The members of this class show a specific H-bond pattern, where two amino H atoms interact with two carboxylic oxygen atoms of two different dipeptides, while the third interacts with a water molecule inside the channel (Fig. S17, ESI†). Notably, L-Phe–L-Val[31] crystallises as an anhydrous crystal form, a not-so common feature for dipeptides.

Conversely, D-Val–L-Phe crystallises as an amphipathic layered structure in a monoclinic unit cell (space group *C*2). To properly describe the self-organisation of D-Val–L-Phe we refer to hydrophilic and hydrophobic regions (Fig. 5 and Fig. S16 in the ESI†). The former is characterised by a H-bond network involving the atoms of the dipeptide backbone and water molecules, while the latter is defined by the hydrophobic side chains. This arrangement is very similar to the solid state assembly of D-Ile–L-Phe dipeptides.[22] Moreover, comparing the

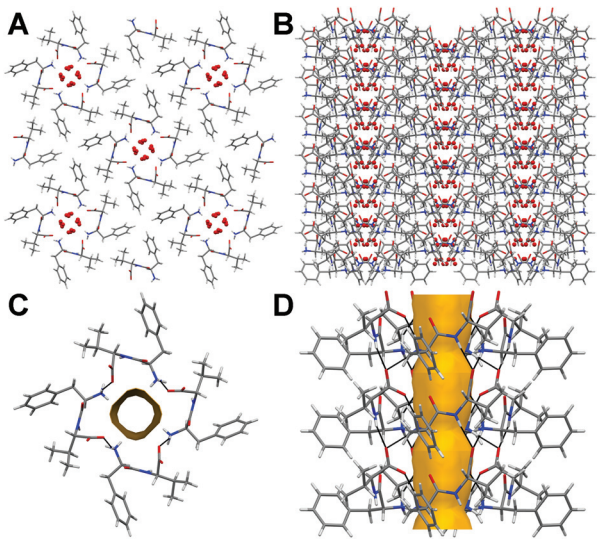

Fig. 4 Single-crystal XRD data for D-Phe–L-Val (CCDC 2160978†). (A and B) Crystal packing along the *c* and *a* axes, respectively. (C and D) Detailed view of the water-channel (gold).

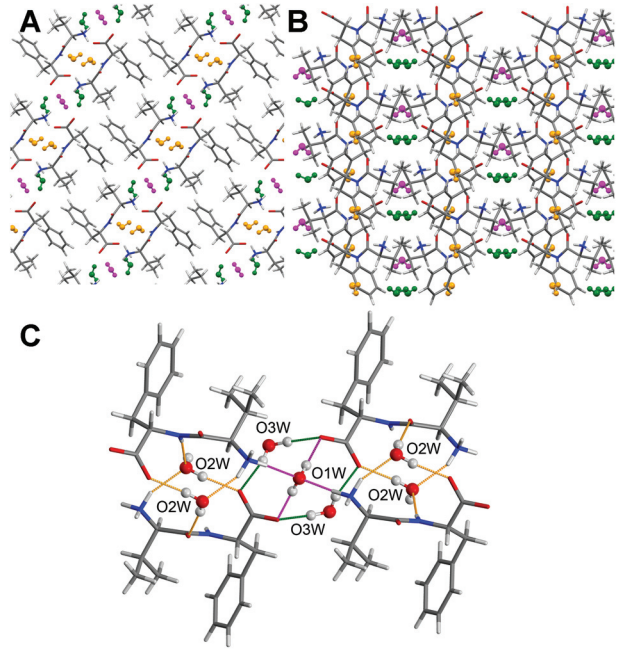

Fig. 5 Single-crystal XRD data for D-Val–L-Phe (CCDC 2160976†). (A and B) Crystal packing along the *b* and *c* axes, respectively. (O1W in magenta, O2W in orange, O3W in green.) (C) Host–guest hydrogen bonds in crystal structure of D-Val–L-Phe (as viewed along the *b* axis).

crystal packing of D-Val–L-Phe with the L-homochiral counterpart, the similarities with the solid state assembly of the dihydrate crystal form are obvious. As for the dihydrate crystal form of L-Val–L-Phe,[31] the NH_3^+ and COO^- hydrogen-bond pattern is missing, all amino H atoms interact with guest water molecules, and the dipeptides organise themselves in a layered structure. Water molecules, aligned along the shortest *b* axis, play a crucial role in the solid state assembly of this dipeptide. To help the reader and simplify the visualisation of the interactions established by water molecules, we decided to depict the guest interactions with different colours (Fig. 5). As can be seen in Fig. 5A and B, O2W (orange) favours the dipeptides' alignment along the direction of the screw axis (interactions depicted in orange), while O1W (magenta) and O3W (green) are directly involved in the solid-state assembly along the *a* axis. In particular, water molecule O1W bridges together four dipeptides acting as an acceptor and donor of H-bonds. The presence of water molecules mediating peptide–peptide interactions is thus confirmed as a distinctive feature of non-gelling dipeptides, in agreement with Leu/Ile analogues.[22,23] The main host–host interaction favours the dipeptides' assembly along the *b* axis. Another weak hydrogen bond can be highlighted between the dipeptides aligned along the screw axis, though its role is secondary considering the importance of the interaction with the water molecule O2W.

Hydrogel biomaterial characterization

Oscillatory rheology confirmed the gel nature solely for samples of D-Phe–L-Val (Fig. 6 and ESI, Section S7†). Time

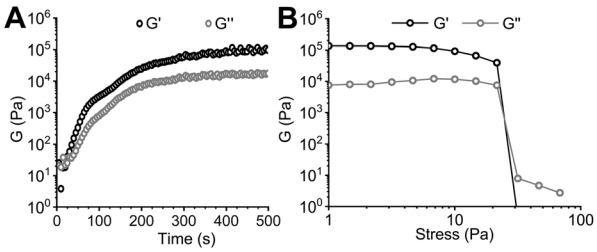

Fig. 6 Oscillatory rheometry time sweep (A) and stress sweep (B) for D-Phe–L-Val.

sweeps confirmed the gelation reached a plateau within 500 seconds, with an elastic modulus G' of $1.23 \pm 0.12 \times 10^5$ Pa, at the mgc of 40 mM (Fig. 6A). Stress sweeps revealed a gel-to-sol transition at 34 ± 8 Pa (Fig. 6B). The hydrogel was thermoreversible (see ESI, Section S8†).

The hydrogel was thus tested for biocompatibility on fibroblast cell culture *in vitro* (Fig. 7). MTT assays in solution revealed no cytotoxicity at concentrations as high as 1 mM (Fig. 7A). The opaque gel was also tested for live/dead fluorescence staining using a microwell assay (Fig. 7B–D). High numbers of proliferative cells were found, with no significant differences in morphology relative to the control. The hydrogel after 24 h partially dissolved and lifted off the plastic, suggesting limited durability under cell culture conditions.

Interestingly, cells were found in high numbers inside the gel, also as it lifted off (Fig. 7D), as they grew preferentially inside its matrix as opposed to the plastic bottom. This finding is highly encouraging in terms of the biocompatibility of this type of scaffold, although for applications it may require enhanced durability.

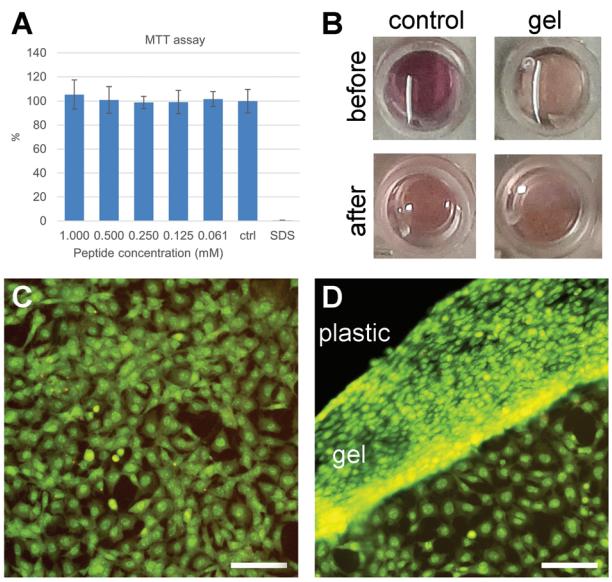

Fig. 7 Cell biocompatibility assays for D-Phe–L-Val. (A) MTT assay. (B–D) Live–dead assay. (B) Photographs of representative Ibidi-μslide wells. (C) Control sample. (D) Hydrogel sample. Scale bar = 100 μm.

Experimental

Materials and methods

Fmoc-amino acids, 2-chlorotrityl resin, and coupling agents were obtained from GL Biochem (Shanghai) Ltd. All other chemicals and solvents were acquired at analytical grade from Merck. NIH3T3 cells were provided by the Life Sciences Dept. of the University of Trieste (Italy). An in-line Millipore RiOs/Origin system provided high-purity Milli-Q-water with resistivity >18 MΩ cm. ^{1}H-NMR and ^{13}C-NMR spectra were recorded on a Varian Innova at 400 MHz and 100 MHz, respectively, with chemical shifts reported as ppm (with tetramethylsilane as internal standard). An Agilent 6120 LC-MS system was used for ESI-MS spectra. Optical microscope images were acquired on a drop of fresh samples deposited on clean glass slides, using a Leitz Labovert instrument with a 20× magnification objective.

Synthetic procedures

Each dipeptide was synthesized by solid phase using standard Fmoc-protection strategy as previously described.[40] Purification was performed on Agilent 1260 using a C-18 column (Kinetex, 5 μm, 100 Å, 250 × 10 mm, Phenomenex), and a mixture of acetonitrile (MeCN) and water with 0.05% TFA (3 ml min^{-1}) as eluent with the following gradients. For D-Phe–L-Val: t = 0 min 15% MeCN, t = 3 min 15% MeCN, t = 16 min 45% MeCN, t = 18 min 95% MeCN. For D-Val–L-Phe: t = 0 min 15% MeCN, t = 3 min 15% MeCN, t = 16 min 55% MeCN, t = 18 min 95% MeCN. The products were lyophilised.

Self-assembly into hydrogels or crystals

Each peptide (40 mM) was dissolved in phosphate buffered saline (PBS, 0.1 M) through heating in an oil-bath at 95 °C for ~15 min, and left to cool down to room temperature.

Circular dichroism

A 0.1 mm quartz cell was used on a Jasco J-815 Spectropolarimeter, with 1 s integrations, 25 accumulations and a step size of 0.5 nm with a bandwidth of 1 nm at 25 °C. Samples were prepared at 1 mM in MilliQ water by adjusting the pH until 7 with NaOH (1 M). Shown spectra are the average of at least 3 measurements.

ATR-IR spectroscopy

Both peptide samples were prepared in PBS as described above at 40 mM on a 1 cm^2 piece of silicon wafer and dried *in vacuo* overnight. ATR-IR spectra were acquired at 4 cm^{-1} resolution, 240 scans, with an ATR-IRAffinity-1S (Shimadzu). Every sample was analysed at least 3 times.

Raman microspectroscopy

Samples were analysed as powders and as prepared in PBS as described above at 40 mM on a microscopy glass slide and dried overnight. Raman spectra were acquired on five different spots per sample with a Invia Renishaw microspectrometer (50) equipped with He–Ne laser at 532 nm (50% power), with 1

accumulation, 1 cm^{-1} resolution. Mapping was performed at 1005 cm^{-1}, 1.3k counts.

Crystallography

Single crystals of D-Phe–L-Val (CCDC 2160978†) and D-Val–L-Phe (CCDC 2160976†) were obtained in PBS at 40 mM after 1 month, and at 100 mM after a few minutes, respectively. For each compound, a single crystal was collected with a loop, cryoprotected by dipping it in glycerol, and then frozen in liquid nitrogen for storage. The crystal was mounted on the diffractometer at the synchrotron Elettra, Trieste (Italy), XRD1 beamline, using the robot available at the facility. The temperature was set at 100 K. Diffraction data were collected by rotating the crystal, using synchrotron radiation with wavelength 0.70 Å. Further details on the structure determination and parameters of the cell unit are in the ESI, Section S6.† Deposition Numbers 2160976 and 2160978† refer to the crystallographic data deposited at the Cambridge Crystallographic Data Centre (CCDC).

Oscillatory rheology

Hydrogels were freshly prepared directly on a 20 mm stainless steel parallel plate of a Kinexus Plus (Malvern). The hot solution was quickly transferred from the oil bath onto the rheometer plate, and the kinetics method set at 25 °C (Peltier) and 1 mm gap was immediately started. Time sweeps were acquired with 1 Pa and 1 Hz, frequency sweeps at 1 Pa and stress sweeps at 1 Hz. Every sample was analysed at least three times and representative measures are shown.

TEM analysis

Samples were prepared as described above at 40 mM, transferred onto TEM carbon grids previously exposed to UV–Ozone Procleaner Plus for 6 min, and dried *in vacuo*. TEM images were acquired on Jeol JEM 2100 (Japan) at 100 kV and analysed with FIJI free software.

Thioflavin T fluorescence

Samples were prepared at different concentrations (see ESI, Section S5†) in PBS inside a Greiner 96 U Bottom Black Polystyrene plate (VWR) (120 µl per well). After 1 hour of assembly, 30 µl of a fresh thioflavin-T solution was added in each well (22 µM in 20 mM glycine-NaOH pH ~ 7.4) and kept in the dark for 15 minutes. Fluorescence was measured (ex. 446 nm, em. 490 nm, 20 nm bandwidth) on an Infinite M1000 pro microplate reader (TECAN) and the experiments were run independently twice in triplicate (n = 6).

Fibroblasts live/dead assay

All the solutions were filtered with a 0.2 µm sterile filter prior to use. The gelator D-Phe–L-Val (20 µl per well) was prepared at 70 mM in 0.01 M PBS, pH-adjusted with NaOH, directly in triplicate wells of a "µ-Slide angiogenesis" treated slide (Ibidi, Germany). After 24 h, 30 µl of media (DMEM + 10% fetal serum albumin, and 2% antimycotic and antibiotic from GIBCO) were added to pre-treat the gel for 1.5 h. Next, the medium was removed and NIH3T3 (fibroblast) cells were added to the gel (10k cells per well, 30 µl media), and cultured at 37 °C, 5% CO_2 for 24 h, by handling the slides according to the manufacturers' instructions. Cell viability was investigated using acridine orange (5 µl per well of a 20 µM solution in 50 mM PBS) and propidium iodide (4 µl per well of a 30 µM solution in 50 mM PBS). After 15 minutes, cells were imaged with a Leica microscope (DFC450C; software LASV4.13) with bright-field and fluorescence green filter (ex. 450–490 nm, em. >520 nm) with 10× and 40× objectives. Each condition was repeated at least in triplicate, and two experiments were performed independently.

MTT assay

NIH3T3 (fibroblast) cells were seeded (10k cells per well) in media (DMEM + 10% FCS, and 2% antimycotic and antibiotic) using 100 µL per well on 96-well microplates (tissue-culture grade, clear, flat bottom, VWR) and incubated overnight at 37 °C and 5% CO_2. The medium was removed and replaced by 100 µL of fresh medium containing the peptide at the desired concentration (serial dilutions of 1 mM). 1% SDS served as positive control (death). Cells were cultured for 24 h. After this time, 10 µL of the MTT labeling reagent (Sigma, 0.5 mg mL^{-1}) were added, and the microplate was incubated for 4 h in a humidified atmosphere (37 °C, 5% CO_2). Next, 100 µL of the solubilisation solution for formazan crystals (4 mM HCl + 0.1% IGEPAL in isopropanol) was added to each well, and the microplate was kept at RT under shaking (Rocker-Shaker MR-12 Biosan, Vetrotecnica) for 30 min. The absorbance was read at 570 nm with a reference wavelength of 690 nm (light scattering) using Infinite M1000-Pro microplate reader (TECAN). Two independent experiments were run in triplicate (n = 6).

Conclusions

This work reveals for the first time that a Phe–Val dipeptide can self-assemble into water-channels and yield a microfibrillar gel with excellent biocompatibility *in vitro*. Until now, unprotected dipeptides' high hydrophilicity was considered a main limitation that hindered assembly of homochiral Val–Phe and Phe–Val, since hydrogelation required more hydrophobic sequences containing at least another carbon atom in the sidechain (*i.e.*, as in Leu/Ile). Interestingly, the hydrogel tested negative for the thioflavin T amyloid stain, despite spectroscopic similarities with other heterochiral hydrophobic tripeptides with amyloid character.

Comparison with non-assembling isomer Val–Phe suggests hydrophobicity *per se* is not the only parameter to enable gelation, since the two isomers display almost identical HPLC R_t. Single-crystal XRD analyses confirmed that only D-Phe–L-Val self-assembled into water-channels whose inner cavity is defined by four peptide molecules connected head-to-tail. The ability to form water-channels is shared with D-Phe–L-Ile and D-Phe–L-Phe gelators, but not with non-gelling D-Ile–L-Phe,

suggesting that the presence of Phe at the N-terminus of these heterochiral dipeptides is a favourable factor. However, D-Phe–L-Val is the first heterochiral dipeptide whose water-channels' inner cavity is defined by 4 peptide molecules, as opposed to the typical 6 in the other cases,[20,22] thus demonstrating that it is possible to attain cavities of different size depending on the peptide sequence (*i.e.*, 0.90 nm for D-Phe–L-Ile, and 0.38 nm for D-Phe–L-Val). This finding is of potential interest to develop supramolecular channels that mediate selective transport of guests through membranes; this is becoming a hot topic for innovative therapies to target diseases as diverse as channelopathies and chronic pain.[43] Besides ion-channels, also water-transport is attracting interest as demonstrated by aquaporin mimicry research for desalination and purification.[44]

Further, the presence of water molecules mediating peptide–peptide interactions appears as a distinctive feature of non-gelling dipeptides, as previously found for tripeptides.[36] Conversely, gelling dipeptides display a continuous network of H-bonds between adjacent amide groups of stacked gelators. Overall, this study confirmed that heterochirality is an effective strategy to attain fibrillation and gelation from otherwise non-gelling dipeptides (*i.e.*, homochiral Phe–Val) into biomaterials with promising biocompatibility profile *in vitro*. As we advance our understanding of the design of these simple biomolecules to form water-channels and hierarchical assemblies into macroscopic and biocompatible soft materials, we anticipate future translation through the incorporation of bioactive sequences to guide cell fate.

Author contributions

Investigation: O. B., G. P., M. P., S. K. Supervision: M. P., P. D'A., C. T., S. M. Writing, initial draft: O. B., G. P. Analysis, writing, review, & editing: all authors. Conceptualization & methodology: C. T., S. M.

Conflicts of interest

There are no conflicts to declare.

Acknowledgements

We acknowledge: Elettra Sincrotrone Trieste for providing access to its synchrotron radiation facilities, G. Bais for assistance with beamline XRD1; the CENN Nanocenter (Slovenia) for access to TEM; the Slovenian Research Agency (RSA – ARRS) through the core funding no. P2-0089 and ARRS projects no. J2-3043, J2-3040, J2-3046, J3-3079.

References

1 A. Lampel, *Chem*, 2020, **6**, 1222–1236.
2 E. R. Draper and D. J. Adams, *Langmuir*, 2019, **35**, 6506–6521.
3 D. J. Adams, *Macromol. Biosci.*, 2011, **11**, 160–173.
4 T. Hu, O. Agazani, S. Nir, M. Cohen, S. Pan and M. Reches, *ACS Appl. Mater. Interfaces*, 2021, **13**, 48469–48477.
5 M. Kurbasic, E. Parisi, A. M. Garcia and S. Marchesan, *Curr. Top. Med. Chem.*, 2020, **20**, 1300–1309.
6 E. R. Cross, S. M. Coulter, S. Pentlavalli and G. Laverty, *Soft Matter*, 2021, **17**, 8001–8021.
7 P. Singh, N. Wangoo and R. K. Sharma, *Soft Matter*, 2020, **16**, 4105–4109.
8 R. Garifullin and M. O. Guler, *Mater. Today Bio*, 2021, **10**, 100099.
9 S. J. Percival, S. Russo, C. Priest, R. C. Hill, J. A. Ohlhausen, L. J. Small, S. B. Rempe and E. D. Spoerke, *Soft Matter*, 2021, **17**, 6315–6325.
10 K. Gayen, S. Hazra, A. K. Pal, S. Paul, A. Datta and A. Banerjee, *Soft Matter*, 2021, **17**, 7168–7176.
11 K. Tao, B. Xue, S. Han, R. Aizen, L. J. W. Shimon, Z. Xu, Y. Cao, D. Mei, W. Wang and E. Gazit, *ACS Appl. Mater. Interfaces*, 2020, **12**, 45192–45201.
12 E. Nikoloudakis, M. Pigiaki, M. N. Polychronaki, A. Margaritopoulou, G. Charalambidis, E. Serpetzoglou, A. Mitraki, P. A. Loukakos and A. G. Coutsolelos, *ACS Sustainable Chem. Eng.*, 2021, **9**, 7781–7791.
13 C. Gila-Vilchez, M. C. Manas-Torres, J. A. Gonzalez-Vera, F. Franco-Montalban, J. A. Tamayo, F. Conejero-Lara, J. M. Cuerva, M. T. Lopez-Lopez, A. Orte and L. Alvarez de Cienfuegos, *Polym. Chem.*, 2021, **12**, 6832–6845.
14 M. C. Manas-Torres, C. Gila-Vilchez, J. A. Gonzalez-Vera, F. Conejero-Lara, V. Blanco, J. M. Cuerva, M. T. Lopez-Lopez, A. Orte and L. Alvarez de Cienfuegos, *Mater. Chem. Front.*, 2021, **5**, 5452–5462.
15 N. A. Dudukovic, B. C. Hudson, A. K. Paravastu and C. F. Zukoski, *Nanoscale*, 2018, **10**, 1508–1516.
16 D. Giuri, L. J. Marshall, C. Wilson, A. Seddon and D. J. Adams, *Soft Matter*, 2021, **17**, 7221–7226.
17 J. Xia, B. Sun, C. Wang, N. Sun, H. Cao, Y. Jia, Y. Yang and J. Li, *J. Colloid Interface Sci.*, 2021, **599**, 661–666.
18 X. Li, Q. Li, J. Fei, Y. Jia, H. Xue, J. Zhao and J. Li, *Angew. Chem., Int. Ed.*, 2020, **59**, 11932–11936.
19 S. Maity, P. Das and M. Reches, *Sci. Rep.*, 2015, **5**, 16365.
20 S. Kralj, O. Bellotto, E. Parisi, A. M. Garcia, D. Iglesias, S. Semeraro, C. Deganutti, P. D'Andrea, A. V. Vargiu, S. Geremia, R. De Zorzi and S. Marchesan, *ACS Nano*, 2020, **14**, 16951–16961.
21 R. F. Silva, D. R. Araújo, E. R. Silva, R. A. Ando and W. A. Alves, *Langmuir*, 2013, **29**, 10205–10212.
22 O. Bellotto, S. Kralj, M. Melchionna, P. Pengo, M. Kisovec, M. Podobnik, R. De Zorzi and S. Marchesan, *ChemBioChem*, 2022, **23**, e202100518.
23 O. Bellotto, S. Kralj, R. De Zorzi, S. Geremia and S. Marchesan, *Soft Matter*, 2020, **16**, 10151–10157.
24 L. Schnaider, S. Brahmachari, N. W. Schmidt, B. Mensa, S. Shaham-Niv, D. Bychenko, L. Adler-Abramovich,

L. J. W. Shimon, S. Kolusheva, W. F. DeGrado and E. Gazit, *Nat. Commun.*, 2017, **8**, 1365.
25 B. Claro, E. González-Freire, M. Calvelo, L. J. Bessa, E. Goormaghtigh, M. Amorín, J. R. Granja, R. Garcia-Fandiño and M. Bastos, *Colloids Surf., B*, 2020, **196**, 111349.
26 S. Fernandez-Lopez, H.-S. Kim, E. C. Choi, M. Delgado, J. R. Granja, A. Khasanov, K. Kraehenbuehl, G. Long, D. A. Weinberger, K. M. Wilcoxen and M. R. Ghadiri, *Nature*, 2001, **412**, 452–455.
27 J. Lerner Yardeni, M. Amit, G. Ashkenasy and N. Ashkenasy, *Nanoscale*, 2016, **8**, 2358–2366.
28 R. Piotrowska, T. Hesketh, H. Wang, A. R. G. Martin, D. Bowering, C. Zhang, C. T. Hu, S. A. McPhee, T. Wang, Y. Park, P. Singla, T. McGlone, A. Florence, T. Tuttle, R. V. Ulijn and X. Chen, *Nat. Mater.*, 2021, **20**, 403–409.
29 N. S. de Groot, T. Parella, F. X. Aviles, J. Vendrell and S. Ventura, *Biophys. J.*, 2007, **92**, 1732–1741.
30 M. Kurbasic, S. Semeraro, A. M. Garcia, S. Kralj, E. Parisi, C. Deganutti, R. De Zorzi and S. Marchesan, *Synthesis*, 2019, 2829–2838.
31 C. Görbitz, *Acta Crystallogr., Sect. B: Struct. Sci.*, 2002, **58**, 512–518.
32 C. Görbitz, *Acta Crystallogr., Sect. C: Cryst. Struct. Commun.*, 2000, **56**, 1496–1498.
33 H. L. Bolt, C. E. J. Williams, R. V. Brooks, R. N. Zuckermann, S. L. Cobb and E. H. C. Bromley, *Pept. Sci.*, 2017, **108**, e23014.
34 N. Amdursky and M. M. Stevens, *ChemPhysChem*, 2015, **16**, 2768–2774.
35 A. M. Garcia, D. Iglesias, E. Parisi, K. E. Styan, L. J. Waddington, C. Deganutti, R. De Zorzi, M. Grassi, M. Melchionna, A. V. Vargiu and S. Marchesan, *Chem*, 2018, **4**, 1862–1876.
36 A. M. Garcia, M. Melchionna, O. Bellotto, S. Kralj, S. Semeraro, E. Parisi, D. Iglesias, P. D'Andrea, R. De Zorzi, A. V. Vargiu and S. Marchesan, *ACS Nano*, 2021, **15**, 3015–3025.
37 V. Castelletto, P. Ryumin, R. Cramer, I. W. Hamley, M. Taylor, D. Allsop, M. Reza, J. Ruokolainen, T. Arnold, D. Hermida-Merino, C. I. Garcia, M. C. Leal and E. Castaño, *Sci. Rep.*, 2017, **7**, 43637.
38 N. Amdursky, Y. Erez and D. Huppert, *Acc. Chem. Res.*, 2012, **45**, 1548–1557.
39 M. Biancalana, K. Makabe, A. Koide and S. Koide, *J. Mol. Biol.*, 2009, **385**, 1052–1063.
40 D. Iglesias, M. Melle-Franco, M. Kurbasic, M. Melchionna, M. Abrami, M. Grassi, M. Prato and S. Marchesan, *ACS Nano*, 2018, **12**, 5530–5538.
41 B. Lekprasert, V. Korolkov, A. Falamas, V. Chis, C. J. Roberts, S. J. B. Tendler and I. Notingher, *Biomacromolecules*, 2012, **13**, 2181–2187.
42 C. H. Görbitz, *Chem. – Eur. J.*, 2007, **13**, 1022–1031.
43 G. Picci, S. Marchesan and C. Caltagirone, *Biomedicines*, 2022, **10**, 885.
44 L.-B. Huang, M. Di Vincenzo, Y. Li and M. Barboiu, *Chem. – Eur. J.*, 2021, **27**, 2224–2229.